SAND2011-4373C

Empirical Battery Model Characterizing a Utility Scale Carbon Enhanced VRLA Battery

Daniel Fregosi
Student Member

Stanley Atcitty
Member

Subhashish Bhattacharya
Member

FREEDM Systems Center
Department of Electrical and Computer Engineering
North Carolina State University
Raleigh, NC
djfregos@ncsu.edu sbhatta4@ncsu.edu

Sandia National Laboratories
Energy Storage and Transmission Analysis
Albuquerque, New Mexico
satcitt@sandia.gov

ABSTRACT

In this paper, the electrical characteristics of a Carbon Enhanced Valve Regulated Lead-Acid Battery from East Penn are investigated and a dynamic model is developed for use in electrical simulations. The electrochemical processes that cause specific dynamic behaviors have been investigated. These processes are explained here, and a non-linear electric model, which captures the results of some of these electrochemical dynamics, is presented. The method to determine model parameters, using experimental data, is shown. To verify the battery model, both a pulsed current profile and an arbitrary current profile were applied to the physical battery and to the battery model and the voltage responses of the two were compared.

I. INTRODUCTION

In this paper, we present an investigation into the electrical characteristics of batteries and the physical phenomena that cause them. The goal is to gain insight on how to design and control systems which utilize lead acid batteries. With better knowledge of the characteristics of the batteries, engineers can interface power electronics with batteries more effectively in order to optimize system configurations and maximize round-trip efficiency, utilization, and lifetime. The characterization procedure outlined here can be easily repeated for other batteries and battery types. Engineers may use this process to develop models of their specific batteries. Such models are useful in simulations and can be embedded in controllers of physical systems for use as an observer.

The Solid State Transformer (SST), which is in development at the NSF FREEDM Systems Center [1], is the specific system which motivates the research from our perspective. The SST is a power electronics interface between the utility distribution grid and distributed energy storage and renewable resources. The SST is a 'plug-and-play' device, meaning there is no special installation required for attaching new sources or storage to the device. We are looking at how to optimally configure and control the system for efficiency and stability. These goals include fast-acting, switching-level control, and long-term, high-level power flow control. The energy storage component of the SST allows for control flexibility. However, for optimization, we must first understand the runtime and dynamic characteristics of the battery.

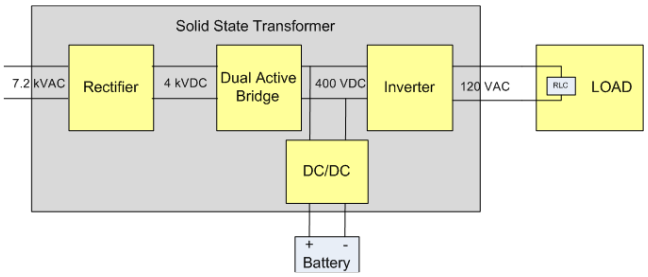

Figure 1. Solid State Transformer Block Diagram

This work focuses on characteristics of lead-acid and valve regulated lead-acid (VRLA) batteries. General characteristics and trends of other battery types can be found in literature [2]. In depth description of VRLA batteries and various explanations of electrochemical phenomena can be found in the "Handbook of Batteries, Third Edition" by Linden and Reddy is a valuable resource [3].

Specifically, the Carbon Enhanced Advanced VRLA Battery from East Penn is modeled in this work. The characteristics included in the model are open circuit voltage,

Sandia National Laboratories is a multi-program laboratory managed and operated by Sandia Corporation, a wholly owned subsidiary of Lockheed Martin Corporation, for the U.S. Department of Energy's National Nuclear Security Administration under contract DE-AC0494AL85000. The work was performed under funding from the DOE Energy Storage Program managed by Dr. Imre Gyuk of the DOE Office of Electricity.

During the academic year, this work was supported by the Department of Defense (DoD) through the National Defense Science & Engineering Graduate Fellowship (NDSEG) Program.

electric resistance, and polarization. Further work can be done to include other characteristics, such as varying capacitance, temperature effects, sulfation, gassing, high depth of discharge damage, and lifetime/aging effects. The process used to characterize the East Penn battery and the general configuration for the battery model circuit has been described previously [4]. The unique work in this project is to characterize a high capacity battery for energy applications, rather than one for portable electronics applications. Furthermore, the characterization done here includes determining model parameters on both the discharge and charge cycle, whereas previous research focuses on the discharge only.

This model accurately captures the runtime characteristics of the VRLA battery. This model is useful in simulations on the order of minutes to days. For studies involving low-level control and battery dynamics, a spectroscopy model is more useful.

In section II of this report, we present the testing, validation, construction, and analysis of the battery model. In the next section, we describe the characteristics of the VRLA battery and how these characteristics were extracted from the testing data. Lastly, in the 'Future Work' section we list battery characteristics that one may wish to add to the model and address ongoing research questions we are investigating.

II. BATTERY MODEL

A. Characterization and Validation Procedure

Figure 2 pictures the test we used to characterize the East Penn Valve Regulated Lead Acid battery. We used an Arbin Instruments SCTS (Supercapacitor Testing System) to discharge and charge a single cell according the current profile shown on the bottom. The tester recorded the voltage at the terminals of the battery with a tolerance of 2.5 mV and a sampling time of 100 ms. We selected the width for each pulse to be 60 minutes with a 50% duty cycle in order to allow the voltage of the battery to relax to a steady state value between pulses. We cycled the cell was cycled from full charge to zero charge and back to full charge. We used specified voltage limits to determine full and empty state of charge of the cell (2.4 V for 100% and 1.75 V for 0%).

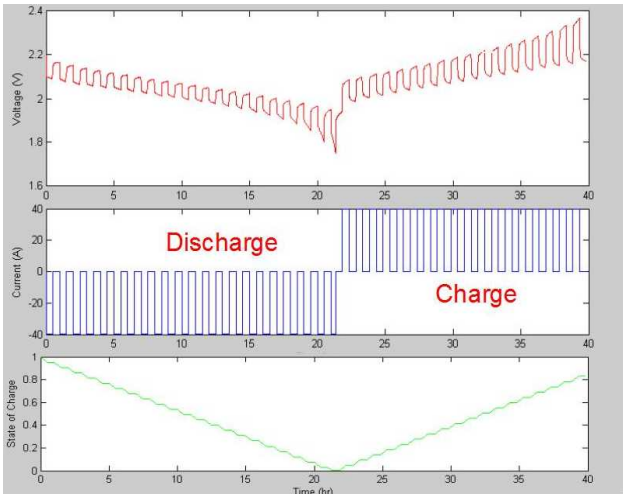

Figure 2. Battery Charictarization Profile (40 A)

For validation of the battery model, we compared the simulated and experimental responses of the cell to two current profiles. Shown in Figure 3 are the cell terminal voltages for both the simulation and the physical battery cell for the 40 A pulse profile. Shown in Figures 4 and 5 are the cell voltages for an arbitrary current profile. The model replicates the battery behavior with an RMS error of less than 1% of the nominal cell voltage of 2V for both profiles. We summarized the validation results in Table I.

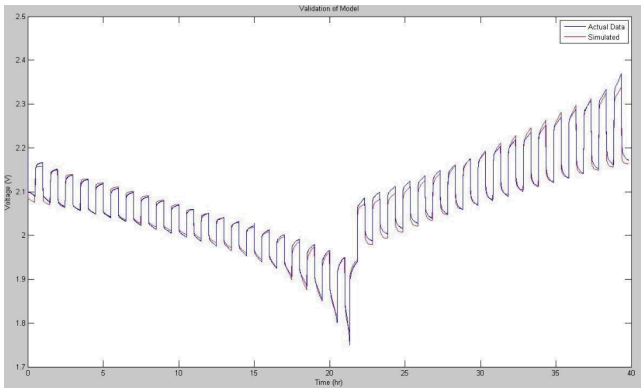

Figure 3. Experimental and Simulated Response on 40 A Profile

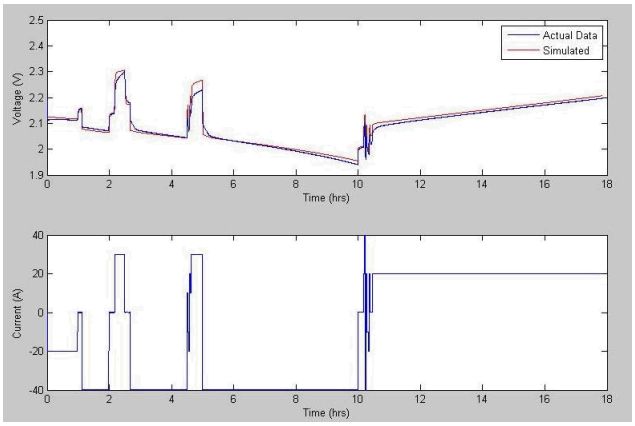

Figure 4. Experimental and Simulated Response on Arbitrary Profile

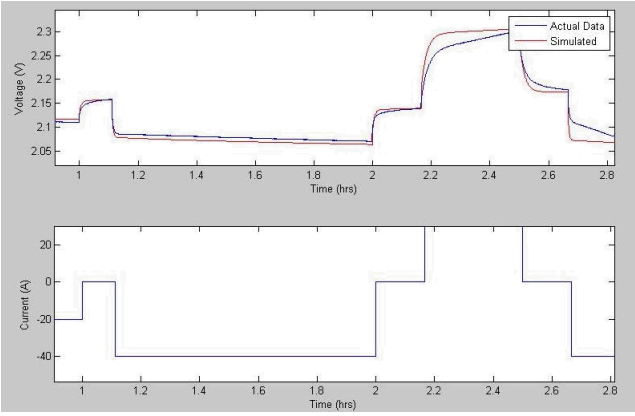

Figure 5. Closer View of Figure 4.

TABLE I. VALIDATION OF BATTERY MODEL

Profile	RMS Error	% of 2V
40 A	7.6 mV	0.38%
Arbitrary	12.1 mV	0.61%

$$RMS\_Error = \sqrt{\frac{\sum (Actual - Simulated)^2}{\#\,Samples}}$$

B. *Model Parameters as a Function of State of Charge*

The equivalent electric circuit battery model is shown in Figure 6. This model is derived from models in previous work [4][5][6]. The battery capacity (runtime) is modeled in the left-hand side of the circuit. The capacity, which was found by integrating the current discharged from the battery during the characterization test, is 433 Ahr. The capacitor on the left hand side of the model is set to 1.56 Mega-Farad, which is the equivalent amp-second value for the measured capacity of the battery. The voltage across this capacitor will vary from one to zero volts as the state of charge varies from 100% to 0%. Therefore, the output of a voltage sensor across the capacitor gives the state of charge. The capacitor is charged and discharged through a dependent current source, which links the two sides of the model. The state of charge value is used by the six function blocks in the center of the model, to determine the values of the circuit elements in the transient model, on the right side.

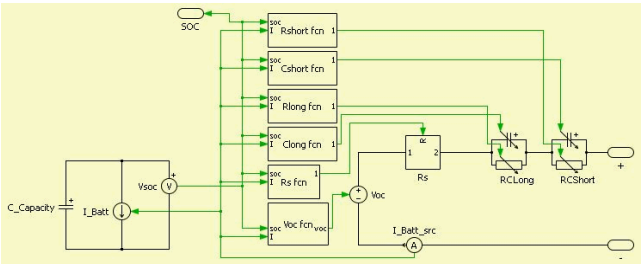

Figure 6. Battery Model Equivalent Circuit

We found each function by fitting curves to empirical data recorded from the characterization test. In the 'Battery Characteristics' section of this report we describe the process of determining these circuit parameters data points from the characterization test. Figures 7, 8, and 9 show the recorded data points for the open circuit voltage, series resistance, and polarization R-C networks, each as a function of state of charge. For each set of data points, we generated a curve to best fit the data, minimizing the square of the difference between each data point and the curve. We list these functions in Table II at the end of this paper.

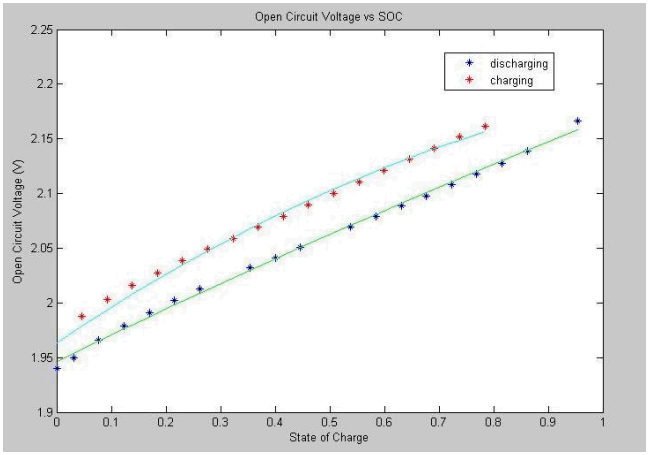

Figure 7. Open Circuit Voltage vs State of Charge

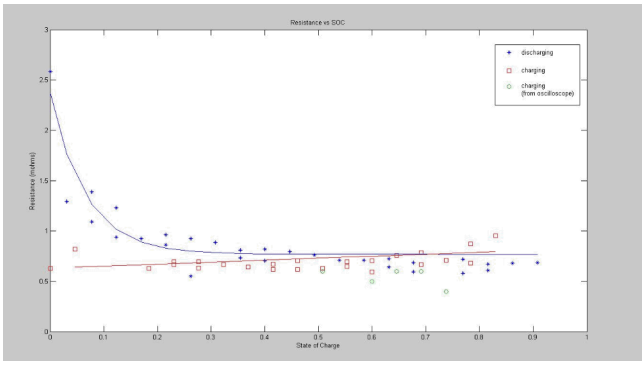

Figure 8. Series Resistance vs State of Charge

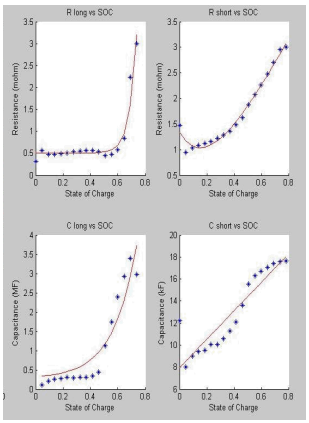

Figure 9. Polarization Parameters vs State of Charge

C. *Analysis of the Dynamics of the Battery Model*

A state space description of the model is given in Figure 10. This description is useful for finding transfer functions and analyzing the eigenvalues of the battery model. This description is for a single cell, where the input to the model is terminal voltage and the output is the cell current. The description could be modified to allow for the current to be an input and the voltage to be an output, if it is needed for a particular application. In this description, the SOC of the cell is held constant.

$$\begin{bmatrix} \dot{V}_{oc} \\ \dot{V}c_{long} \\ \dot{V}c_{short} \end{bmatrix} = \begin{bmatrix} 0 & \frac{-1}{R_{series}*C_{long}} & \frac{-1}{R_{series}*C_{short}} \\ \frac{-1}{R_{series}*C_{long}} & \frac{-1}{R_{series}*C_{long}}+\frac{-1}{R_{long}*C_{long}} & \frac{-1}{R_{series}*C_{short}} \\ \frac{-1}{R_{series}*C_{short}} & \frac{-1}{R_{series}*C_{short}} & \frac{-1}{R_{series}*C_{short}}+\frac{-1}{R_{short}*C_{short}} \end{bmatrix} * \begin{bmatrix} V_{oc} \\ Vc_{long} \\ Vc_{short} \end{bmatrix} + \begin{bmatrix} 0 \\ \frac{-1}{R_{series}*C_{long}} \\ \frac{-1}{R_{series}*C_{short}} \end{bmatrix} * V_{cell}$$

$$[I_{cell}] = \begin{bmatrix} \frac{-1}{R_{series}} & \frac{-1}{R_{series}} & \frac{-1}{R_{series}} \end{bmatrix} * \begin{bmatrix} V_{oc} \\ Vc_{long} \\ Vc_{short} \end{bmatrix} + \begin{bmatrix} \frac{1}{R_{series}} \end{bmatrix} * V_{cell}$$

Figure 10. State Space Description of Battery Model

We analyzed the impedance of the battery as a function of both state of charge and frequency. The impedance of the battery is relevant for studies involving the dynamic performance of the battery. This analysis could be used for system design and control to optimize response time and efficiency. It is noted that impedance spectroscopy tests are utilized to capture similar information; therefore we plan to also incorporate spectroscopy data into our research in the future. In Figure 10, we show three curves of the impedance of the battery cell for a range of frequencies (10^-5 Hz to 1 Hz). A single curve shows the impedance of a cell for this range of frequencies for a single state of charge. Shown are curves for 70%, 50%, and 30% SOC. The horizontal axis represents the resistance and the vertical axis represents the negative reactance, similar to a spectroscopy plot. The battery behaves more like a capacitor at certain frequencies. For each curve, the resistance of the battery decreases as the frequency of the perturbations increase. The same information is presented in Figure 11 in the form of a bode plot. The curves range from 10^-10 Hz to 1 Hz. The family of curves represents different cell SOC values, ranging from 10% to 100% in increments of 5%.

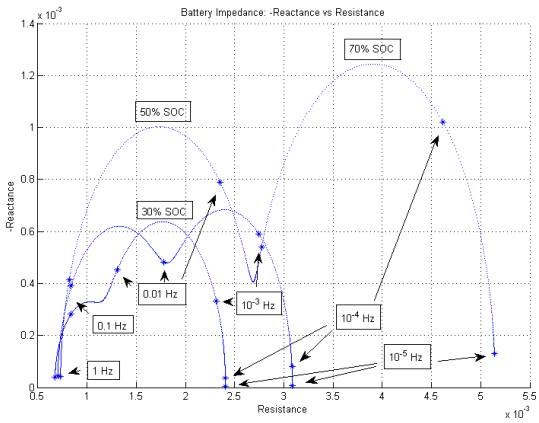

Figure 11. -Reactance vs Impedance. Each curve is for a different State of Charge and each point is for a different frequency.

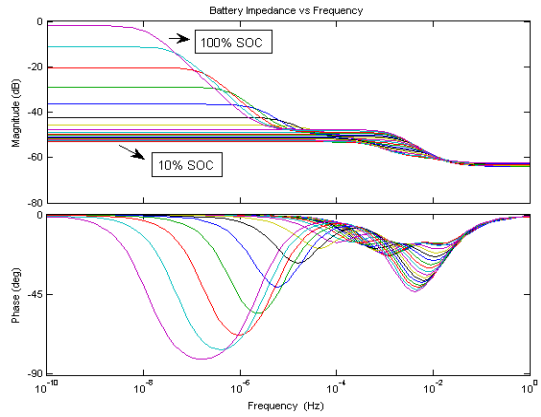

Figure 12. Battery Impedence vs Frequency. Each line is for a different SOC, ranging from 10% to 100%

It is important to note that some of the characteristics of these impedance plots likely come from the specific battery model which we used. We used a model with two R-C branches. In the impedance representations in figures 10 and 11, there are two inflection points where the battery behaves somewhat like a capacitor, corresponding to the number of R-C parallel branches we used to characterize the battery. An arbitrarily high number of R-C branches could be used to characterize the battery to an arbitrarily high degree of accuracy. The method we used is not necessarily the best method for capturing high frequency impedance information on the battery. For this reason, impedance spectroscopy is preferred. This model is more useful for runtime analysis.

III. BATTERY CHARACTERISTICS

A. *Open circuit voltage*

The open circuit voltage of the battery is the voltage that is present regardless of whether current is present. This voltage is one of several components that contribute to the terminal voltage whenever there is current in the battery. However when there no current in the battery and the battery

has reached steady state, this voltage is the only component which contributes to the terminal voltage.

The voltage waveform in Figure 13 is taken during the discharge cycle of the battery. For the period between 0.5 and 1 hr, there is not current being drawn from the battery. At the end of the window, the battery voltage reaches a steady state value, which is the open circuit voltage. The open circuit voltage was taken at the steady state point for each curve in which no current was present in the battery. These values are separated between points taken during the discharge cycle and points taken during the charge cycle, and they are plotted in Figure 7.

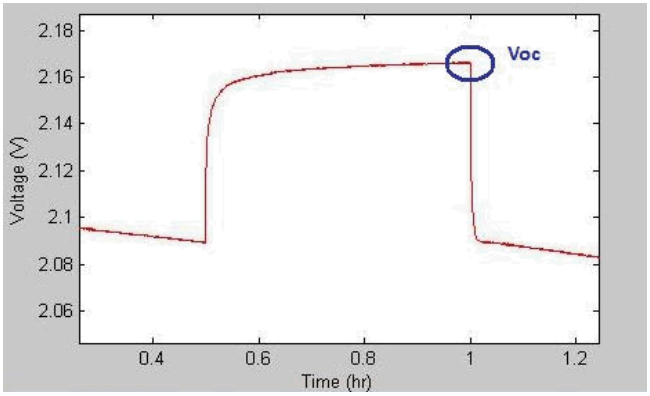

Figure 13. Indication of point on characterization profile where Voc is recorded

Two polynomial functions of the state of charge were fit to the data points for the discharging and the charging cycles. These functions are incorporated into the battery model. When the polarity of battery current corresponds to discharging of the battery, the discharging polynomial function is used to determine the open circuit voltage of the model. Likewise, when the polarity of current corresponds to charging the battery, the charging polynomial is used to determine the open circuit voltage. The hysteresis effect of the open circuit voltage has been described and modeled in previous work, thus this result is expected.

B. Electric resistance

The electric resistance of the battery can be detected instantaneously whenever current is either applied or removed from the battery. On the voltage waveform in Figure14, no current is present between the 0.5 hr and 1 hr marks. There is an immediate voltage rise and drop whenever the current is removed and then applied again.

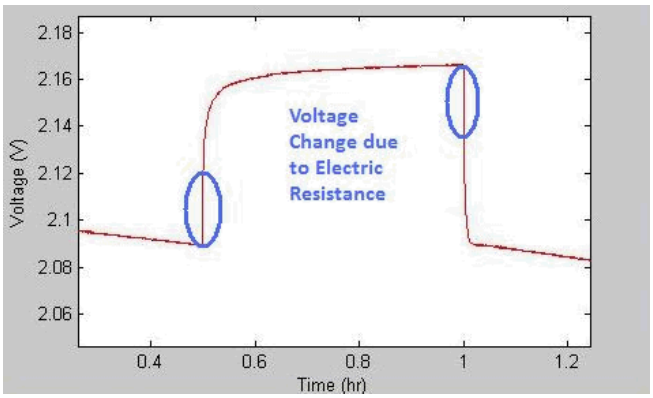

Figure 14. Indication of Series Resistance Effect on Charictarization Profile

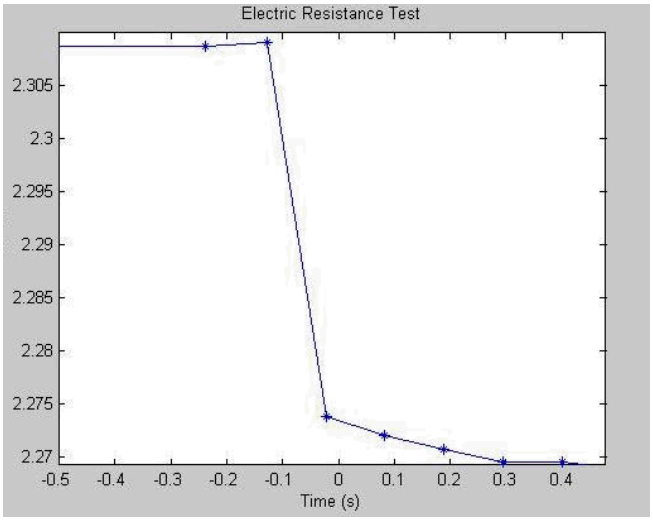

Figure 15. Voltage Drop due to Series Resistance – time value in seconds

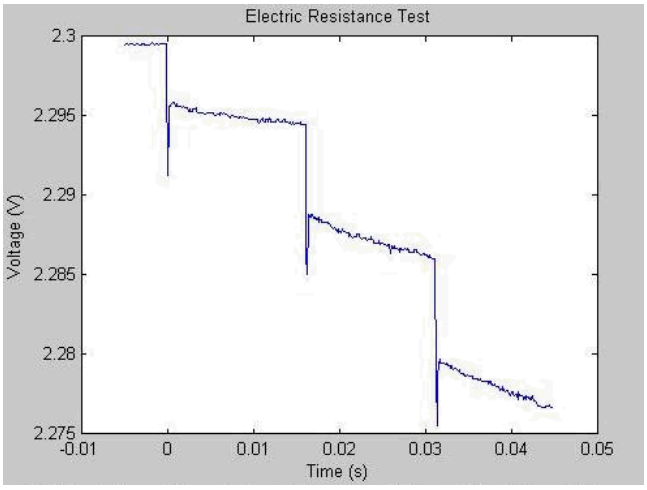

Figure 16. Voltage Drop Due to Series Resistance – time value in milli-seconds

This effect can be differentiated from the voltage relaxation effect which is caused by ionic polarization since the electrical effect can be seen immediately while the

electrochemical effect happens more gradually. The accuracy of measuring the resistance depends on the sampling time of the voltage sensor. The two graphs above help illustrate this. Figure 15 shows the voltage profile at a sampling interval of 100 ms from the Arbin tester. Figure 16 shows the same voltage profile, sampled at 100 us from an oscilloscope. The step changes seen in the lower graph are due to the channels of the tester not being absolutely synchronized. The current goes from 40 A to 0 A in steps of 10 A. These steps are 15 to 20 ms apart, and a tester which samples every 100 ms may capture a terminal voltage at an instant when the current is 10, 20, or 30 A. To isolate the electric resistance from other effects of the test, the instantaneous voltage drop due to a change in current must be isolated. Dividing the voltage change by the change in current gives this resistance. It can be seen on Figure 16, taken from the oscilloscope that the voltage drop happens within milliseconds. As the test continues, the open circuit voltage and voltage relaxation effects contribute significantly to the terminal voltage. Therefore, a tester with a short sampling time will be more accurate. An inductive characteristic was found in looking at the oscilloscope voltage waveform. This characteristic is not included in the model.

Since taking readings from the oscilloscope is not automated and the discharge and charge lasts on the order of days, is it preferred to use data from the automated Arbin tester. On Figure 8, the star and square data points are the resistance values calculated from data captured by the Arbin tester. The circular data points are resistance values calculated from data taken by an oscilloscope. The accurate, circular, resistances are calculated from data taken during the charging cycle, and should be compared with the square resistance values. The more accurate resistance values verify that the values calculated from the Arbin tester are accurate enough for the purposes of this model. Repeating the process for modeling the open circuit voltage, two functions were fit to the data, one for charging and one for discharging. These functions were incorporated to the model to determine the resistance at a given state of charge and current polarity. A variable resistor is used in the transient side of the model to create the electric resistance effect.

C. Polarization/Voltage Relaxation

The polarization effect occurs as concentrations of the ions in the electrolyte near the plates change based on the reactions at the plates. The electric potential of the reaction at each plate is determined by the concentration of the ions near the plate. The Nernst Equation describes how the electric potential varies as a function of ion concentrations. As the ions are either produced or consumed by the plate, depending on the whether the plate is being oxidized or reduced, an excess or a scarcity of ions are found near the plate. The diffusion of ions across the electrolyte solution balances this effect, and an equilibrium is eventually reached to where the plates produce or consume ions at a rate equal that of the ions diffusing from the electrolyte solution to an area near the plates. During this process, the ion concentration of the overall solution changes, which affects the terminal voltage. However, the voltage effect of the ion concentration as a whole varying is captured by the open circuit voltage component of the model. The process that occurs when no current is being cycled through the battery, and no chemical reaction is happening, is that the ion concentrations near the plates are equalizing with the concentration of the solution as a whole. This can be seen as a 'voltage relaxation' at the terminals. Both processes occur over the span of minutes. For this test, it was assumed that the steady state condition is reached in 30 minutes, thus the current pulses were set to duration of 30 minutes with 30 minutes of no current between pulses.

In modeling this effect, capturing the electrochemical phenomena is not attempted. An attempt to capture only the electrical dynamics of these phenomena is made. The voltage relaxation curves from the entire profile were separated into four types. During the discharge cycle, the two types of relaxation are that during a pulse of current and that during a period of no current. Likewise, there are two types of relaxation curves during the charge cycle. As shown in the picture below, these curves were separated and plotted according to their type. The voltage relaxation effect was isolated from the electric resistance and the open circuit voltage effects. The resistance effect was removed by taking out the initial voltage rise/drop at the start of each curve. The open circuit voltage effect was removed by subtracting the open circuit voltage value corresponding to each specific state of charge value (by using the functions found previously for Voc vs SOC) from the waveforms at each data point. This moved the start of each relaxation curve to 0V. For the two curve types in which no current is present, the state of charge remains constant and a single voltage is subtracted from each data point over the entire length of each curve. For the other two types where current is present, the state of charge changes over the length of the relaxation curve. The open circuit voltage was calculated as a function of the state of charge for each specific data point and then subtracted from each point on each relaxation curve, in order to remove this phenomenon which is captured in another part of the model (described previously). The voltage relaxation curves, isolated from the open circuit voltage and electric resistance effects, are shown in Figure 17.

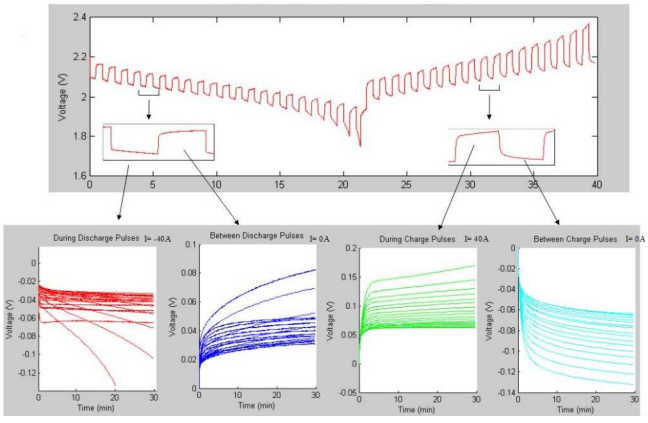

Figure 17. Four Families of Polarization Curves – Normalized to 0 V

Each relaxation curve was fit to an exponential function. The function includes a short and a long time constant, with two parameters characterizing each exponential curve. The form of the equation is:

$$V = K_1 - K_2*\exp(-K_3*t) - K_4*\exp(-K_5*t)$$

For the complementary curves in the discharge/charge cycles, the polarity of the exponential functions is reversed. The circuit in the battery model is designed to reproduce this behavior with two parallel RC networks. The process of fitting the voltage relaxation to an RC network is well explained in previous work [6]. With a step change in current, the circuit in the model responds according to:

$$V = V_0 - R_{short}*\exp(-R_{short}*C_{short}*t) - R_{long}*\exp(-R_{long}*C_{1ong}*t)$$

The elements in the circuit which model the polarization effect do not represent physical resistors and capacitors in the battery, but they serve to empirically produce the voltage relaxation waveforms which occur as a result of electrochemical processes. Each relaxation curve was fit with a function of the form shown above. The parameters of each function were then plotted versus the state of charge at the beginning of each curve. Another curve fit was performed for each parameter as a function of state of charge. This process was repeated for all four curve types. The initial curve fitting for the relaxation curves with no current present during the charging cycle is shown in Figure 18. The parameters are then taken as functions of state of charge. The curve fitting functions for these parameters was shown previously in Figure 9.

In the circuit model, the two resistors and capacitors are variable circuit elements. Their value is calculated by function blocks which implement the functions found by the parameter value versus SOC curve fitting process. For each of the four circuit elements, four functions are included in the model to compute the element's value based on whether the battery is charging or discharging and whether or not current is present in the battery, reproducing the four types of relaxation curves.

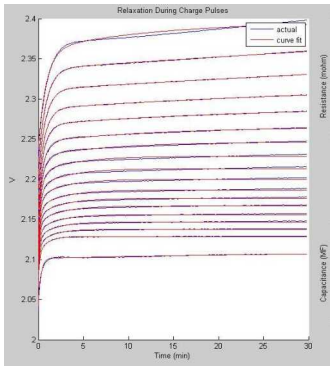

Figure 18. Voltage Relaxation Curves with Best Fit Lines

IV. Future Work

A. *Expansion of model*

Additions could be made to the model of the East Penn VRLA battery. Several characteristics were not included in the battery model that may be significant for a particular application. For example, other research suggests that the polarization parameters change based on the level of current in the pulse [7]. Depending on the application of the model, one may include effects due to variation in temperature, capacity as a function of charge and discharge rate, capacity as a function of number of cycles, sulfation, gassing, or other aging effects like damage caused by high depth of discharge.

As mentioned previously, we are currently working on incorporating spectroscopy measurements into the battery model, to make the model more versatile and to gain a better understanding of the dynamics of the battery.

B. *Applications*

As mentioned briefly in the introduction, we are using the runtime model to investigate and compare algorithms where the battery is used to smooth intermittent sources. There are various algorithms that can be used to limit the ramp rate of power sent to the grid from the intermittent source. This model can be utilized to compare the efficiencies of different algorithms. The model is also useful for investigating the sizing requirements for different smoothing algorithms.

It is of interest to compare the runtime model of this East Penn VRLA battery to models of other battery technologies. We have plans to characterize Lithium Ion batteries. When each type of battery is characterized using the same procedure, merits can be assigned based on common performance measurements. For example, the efficiency of a battery module can be measured for a smoothing application for a given PV power profile.

Lastly, this model can be used to investigate system configuration optimization. Research shows that some ramp rate control can be realized with the use of electrochemical capacitors (EC) instead of batteries [8]. In evaluating alternative system configurations, an economic function can be developed which includes energy efficiency, storage capabilities, reliability, lifetime, and system cost.

Battery Model Functions

TABLE II. Equations and Conatants for Battery Model Parameters as a Function of State of Charge

Open Circuit Voltage	
While Charging	While Discharging
Voc = k1(1) + soc*k1(2) +soc^2*k1(3)	Voc = k2(1) + soc*k2(2) +soc^2*k2(3)
k1 = [1.963 0.334 -0.113]	k2 = [1.946 0.242 -0.0218]
Series Resistance	
While Charging	While Discharging

Rs = k3(1) - k3(2)*soc	Rs = k4(1) - k4(2)*exp(-k4(3)*soc)
k3 = [0.000625 -0.000147]	k4 = [0.000729 -0.00164 15.95]
Long Time-Constant Capacitor	
While Charging/Relaxation	While Charging/Active
Clong = k5(1) - k5(2)*soc	Clong = k6(1) + k6(2)*exp(k6(4)*soc - k6(3))
k5 = [652000 286000]	k6 = [302000 54400 0.251 5.962]
While Discharging/Relaxation	While Discharging/Active
Clong = -k7(1)*(k7(2)*soc - k7(3))^2 + k7(4)	Clong = k8(1) + k8(2)*exp(k8(3)*(0.8 - soc))
k7 = [5540000 1.0378 0.535 2200000]	k8 = [-3594000 8810000 -1.068]
Short Time-Constant Capacitor	
While Charging/Relaxation	While Charging/Active
Cshort = k9(1) + k9(2)*soc	Cshort = k10(1) - k10(2)*soc
k9 = [12300 8960]	k10 = [7960 -12870]
While Discharging/Relaxation	While Discharging/Active
Cshort = k11(1) - k11(2)*soc	Cshort = k12(1) - k12(2)*soc + k12(4)*(1.5*soc-k12(3))^2
k11 = [10800 -22800]	k12 = [8710 -2080 1.135 10000]
Long Time-Constant Resistor	
While Charging/Relaxation	While Charging/Active
Rlong = k13(1) + k13(2)*soc	Rlong = k14(1) + k14(2)*exp(k14(4)*soc-k14(3))
k13 = [0.000583 0.000477]	k14 = [0.000516 0.00490 16.565 21.65]
While Discharging/Relaxation	While Discharging/Active
Rlong = k15(1) + k15(2)*exp(-k15(3)*soc) + k15(4)*soc	Rlong = k16(1) + k16(2)*exp(-k16(3)*soc)
k15 = [0.000224 0.000973 8.46 0.000137]	k16 = [0.000142 0.0167 17.3]
Short Time-Constant Resistor	
While Charging/Relaxation	While Charging/Active
Rshort = k17(1) + k17(2)*exp(k17(3)*soc)	Rshort = k18(1) + k18(2)*exp(-k18(3)*soc) + k18(4)*soc
k17 = [0.000689 0.000107 3.33]	k18 = [-0.000946 0.00228 4.15 0.00502]
While Discharging/Relaxation	While Discharging/Active
Rshort = k19(1) + k19(2)*exp(-k19(3)*soc) + k19(4)*soc	Rshort = k20(1) + k20(2)*exp(-k20(3)*soc) + k20(4)*soc
k19 = [-0.0000007 0.0008 6.14 0.00077]	k20 = [-0.00398 0.00478 1.15 0.00379]

ACKNOWLEDGMENT

The authors would like to acknowledge the FREEDM Systems Center for providing laboratory and office facilities. The FREEDM Systems Center is supported by the ERC Program of the National Science Foundation under Award Number EEC-0812121. The authors also acknowledge East Penn for the donation of battery cells.

REFERENCES

[1] Z. Tiefu, Z. Jie, S. Bhattacharya, M. Baran, and A. Huang, "An average model of solid state transformer for dynamic system simulation." Power & Energy Society General Meeting. (2009): 1-8.

[2] Masters, Gilbert M.. *Renewable and Efficient Electric Power Systems.* Hoboken, NJ: John Wiley & Sons, Inc., 2004. 557-572. Print

[3] Linden, David, and Reddy Thomas B. *Handbook of Batteries.* 3. Mcgraw-Hill Handbooks, 2001

[4] M. Chen and G. Rincón-Mora, "Accurate Electrical Battery Model Capable of Predicting Runtime and I-V Performance", *IEEE Transactions on Energy Conversion*, vol. 21, no. 2, pp. 504-511, June 2006

[5] B. Schweighofer, K.M. Raab, and G. Brasseur, "Modeling of High Power Automotive Batteries by the Use of an Automated Test System", *IEEE Transactions on Instrumentation and Measurement*, vol. 52, no. 4, pp. 1087-1091, August 2003

[6] S. Tian, M. Hong, and M. Ouyang, "An Experimental Study and Nonlinear Modeling of Discharge I-V Behavior of Valve-Regulated Lead-Acid Batteries", *IEEE Transactions on Energy Conversion*, vol. 24, no. 2, pp. 452-457, June 2009

[7] N. Kakimoto, H. Satoh, S Takayama, and K Nakamura, "Ramp-Rate Control of Photovoltaic Generator With Electric Double-Layer Capacitor", *IEEE Transactions on Energy Conversion*, vol. 24, no. 2, pp. 465-473, June 2009